Supporting Information for:

Structural Evidence of Amyloid Fibril Formation in the Putative Aggregation Domain of TDP-43

Miguel Mompeán[1,*] Rubén Hervás[2], Yunyao Xu[3], Timothy H. Tran[4], Corrado Guarnaccia[5], Emanuele Buratti[5], Francisco Baralle[5], Liang Tong[4], Mariano Carrión-Vázquez[2], Ann E. McDermott[3], and Douglas V. Laurents[1,*]

1 Instituto de Química Física Rocasolano , CSIC Serrano 119, 28006 Madrid, Spain
2 Instituto Cajal, IC-Consejo Superior de Investigaciones Científicas Avda. Doctor Arce 37, E-28002 Madrid, Spain & Instituto Madrileño de Estudios Avanzados en Nanociencia (IMDEA-Nanociencia). E-28049 Cantoblanco, Madrid, Spain.

3 Department of Chemistry, Columbia University, New York, New York 10027, USA
4 Department of Biological Sciences, Columbia University, New York, New York 10027, USA.
5 International Centre for Genetic Engineering and Biotechnology, I-34149 Trieste, Italy

*To whom correspondence may be addressed:

Telephone: +34 91-745-9543

Fax: +34 91-564-2431

Email: mmompean@iqfr.csic.es, dlaurents@iqfr.csic.es

CONTENTS:

SI Methods

Circular Dichroism: Secondary Structure Analysis.
Estimations of secondary structure content were performed using the CDSSTR algorithm (1), as implemented on the webserver Dichroweb***:*** ***http://www.cryst.bbk.ac.uk/cdweb*** (2,3)

NMR Spectroscopy analysis of the longer peptide TDP-43 (322-366)
The peptide TDP-43(322-366) was synthesized by standard solid phase methodology and purified at the ICGEB, Trieste. It was dissolved in aqueous buffer containing 100% D_2O for the 2D ^{1}H-^{13}C HSQC spectrum or alternatively 90% H2O/10% D2O for the 1D 1H, ^{1}H 2D ^{1}H TOCSY and NOESY spectra. Both samples contained 1 mM deuterated acetic acid and the pH was 6.0. All spectra were recorded 5ºC on a Bruker 600 MHz NMR spectrometer equipped with a cryo probe and z-gradients. For the TOCSY and NOESY spectra, mixing times of 60 ms and 150 ms were used, respectively, and the matrix was 2k x 512. The spectra were acquired and processed using the Bruker program Topspin version 2.1.

Molecular Dynamics (MD) and Replica-Exchange MD (REMD) Simulations

All the simulations were performed using the amber99sb-ildn force field parameters (4) as implemented in the GROMACS package (5), version 4.5.5. The choice of this force field was based on previous satisfactory results describing amyloid-like systems (6,7). The systems were placed in TIP3P water (8) cubic boxes, leaving at least 1.2 nm between each solute atom and box edges. After steepest descent energy minimization, two equilibration periods were performed restraining the protein atoms movement, to allow solvent molecules equilibrate around the solute (500ps, NVT and 2ns NpT). The Berendsen (9) weak coupling scheme was used during these periods. For the MD data collection stage, we used the Nosé-Hoover (10) thermostat and Parrinello-Rahman (11) barostat in absence of any restraints, with time constants of 0.5 and 1.0 ps, respectively. The LINCS algorithm (12) was applied in all the simulations to allow a time step of 2 fs. All the individual runs ranged from 100 to 110 ns. The peptide model included N-terminal acetyl and C-terminal amide groups to avoid artificially favoring β-hairpin

formation through attractive electrostatic interactions. To ensure the independence of the simulations, we used different initial velocities in each run. The short-range nonbonded interactions were cut-off at 1 nm, while long-range electrostatics were calculated with the particle mesh Ewald (PME) algorithm (13). Dispersion-correction was applied to account for van der Waals interactions at distances longer than the cut off, and periodic boundary conditions were applied in all directions. The peptide models were built using PyMOL (http://www.pymol.org/).

Protein-Protein Docking

Docking of two ten-stranded systems was performed with the HADDOCK (14) program, using data from solvent accessible surface (SAS) calculations. The HADDOCK program was used to generate the twenty-stranded oligomer with sidechain intermeshing (dry interface), made up by a pair of pentamer TDP-43 (each sheet contains five β-hairpins and thus ten β-strands). The residues with high solvent accessibility (>45%) were selected as active residues and the neighbors of these active residues were selected as passive residues. After rigid body-energy minimization, the best 200 solutions based on the inter-molecular energy were selected for the semiflexible docking, followed by explicit water solvation. The top 200 docked models were clustered by a cutoff of 3.5 Å, with a minimum of 10 structures in each cluster, which yielded six clusters. In terms of HADDOCK score and total energy, the best 10 structures from the first cluster were selected as the final model for the TDP-43 (341-357) oligomer.

Supporting Figures

The NMR spectra of the TDP-43 (322-366) show poor chemical shift dispersion, which is typical of random coil ensembles. In a previous study of the shorter peptide TDP-43 (342-366), the NMR signals were assigned unambiguously and this segment was determined to exist (prior to aggregation) as a random coil (Mompean *et al.* (2014) ABB). Here, we find no significant chemical shift differences for the signals arising from residues 342-366 in the shorter peptide compared to the longer peptide spanning residues 322-366. This is strong evidence that this segment still exists initially as a random coil ensemble in the context of the longer 322-366 peptide. The longer peptide contains many Ala (7) and Met (5) residues which we could not assign individually due to strong overlap. This lack of dispersion and the chemical shift values of the overlapped Ala and Met resonances are consistent with a random coil ensemble containing a minor (<25%) population of helical conformers.

The sole Trp residue at position 334 was completely assigned. Its chemical shift values (in ppm): H=8.17, Hα=4.63, Hβ2=3.32, Hβ3=3.27, Hδ=7.20, HNε=10.21, Hε3=7.48, Hζ2=7.48, Hζ3=7.10, Hη2=7.25, Cα=57.4, Cβ=29.4, are all close to those observed for Trp residues in short, unstructured peptides. Furthermore, we observe no NOE signals between the aromatic Trp H and Gln 327 or with aliphatic H from other residues in this polypeptide.

1D ^{1}H NMR spectra recorded confirm that the TDP-43 (322-366) concentration was unchanged and that no aggregation occurred during the acquisition of these 2D spectra (18 h); conditions in which TDP-43 (341-366) and TDP-43(341-357) do extensively aggregate and lose most of their NMR signal intensity. The TDP-43 (322-366) sample did partially precipitate after 40 h. Taking these findings into account, we conclude that flanking segments do not promote the aggregation of TDP-43 (341-357).

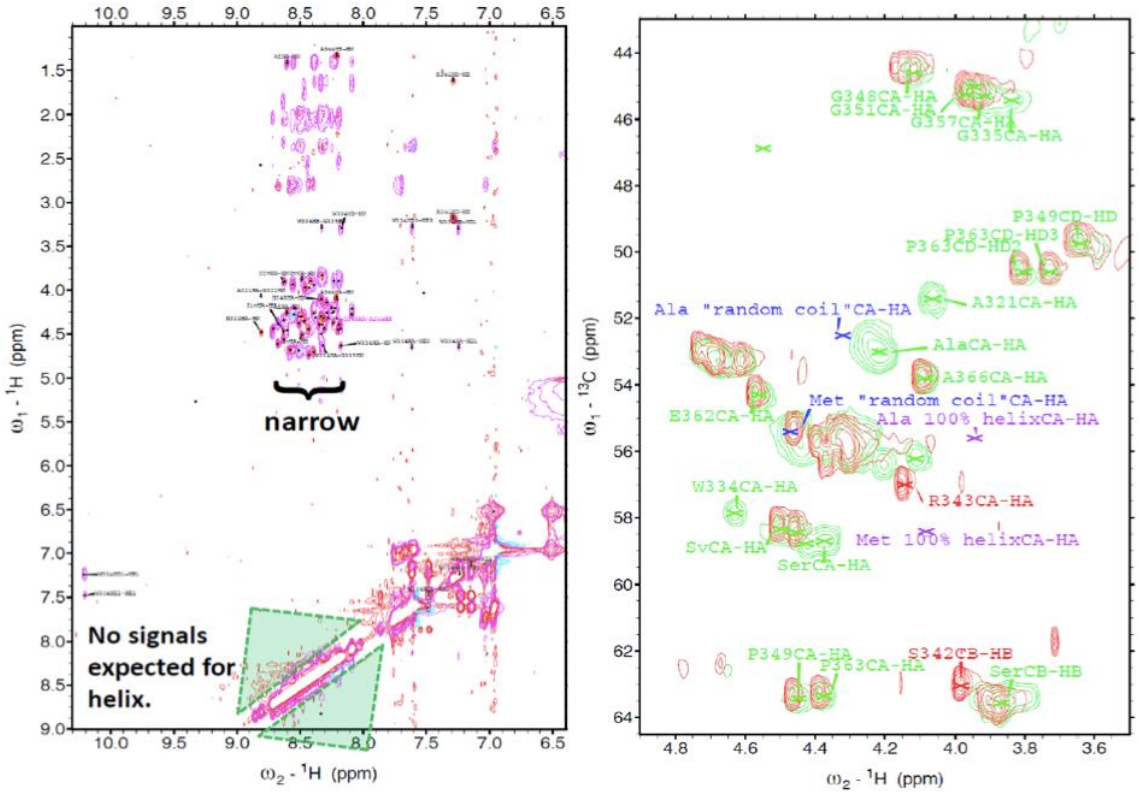

Figure S1: NOESY (***left panel***) and ^{1}H-^{13}C HSQC (***right panel***) NMR spectra of TDP-43 (322-366). Downfield region of the 2D ^{1}H NOESY NMR spectrum of TDP-43 (322-366) (***left***). The narrow chemical shift dispersion of the ^{1}HN signals (<1 ppm) is evident. The region where $^{1}HN_{i}$ to $^{1}HN_{i+1}$, $^{1}HN_{i+3}$ and $^{1}HN_{1+4}$ NOE signals characteristically appear in helical peptides and proteins is indicated. No such signals are observed here. The alpha region of the ^{1}H-^{13}C HSQC spectra of TDP-43(322-366) (in **green**) and TDP-43 (342-366) Q343R variant (in **red**) (***right***). Some nuclei are labeled. "X's" mark the expected chemical shifts values of Ala and Met HC alpha signals in random coil (**blue**) or 100% helical (**purple**) conformations. It is clear that the group of overlapped Ala peaks is much closer to the position expected for random coil than to that expected for helix.

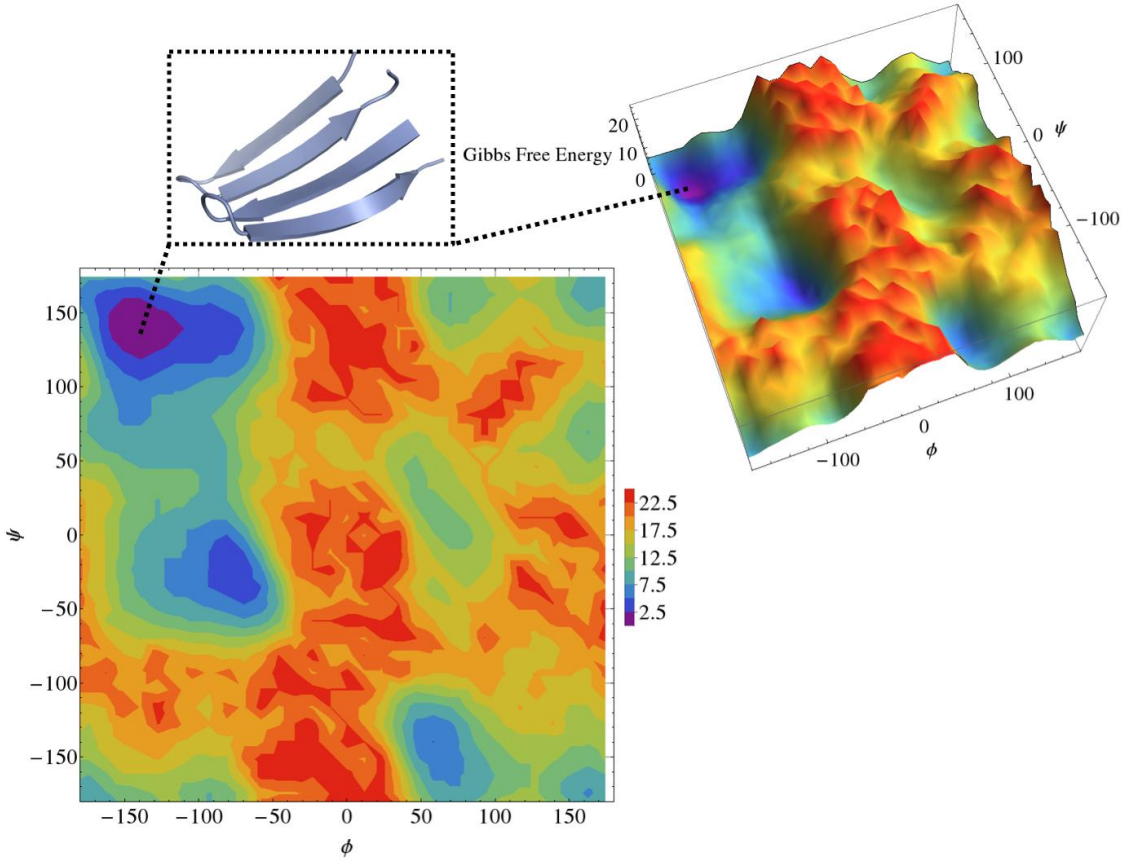

Figure S2: Free Energy Landscapes in the phi and psi dihedral angle space. The phi and psi torsion angles were extracted from the trajectory of a REMD simulation of two TDP-43 dimers with the starting configuration used for the MD runs. The free energy landscape in this set of angles was built from the g_sham utility implemented in GROMACS. The time of the trajectory at which this minimum occurs can be obtained directly from the coordinates (phi and psi) of this point, which is equivalent to an ***in-register,*** lateral association. Since these angles define the secondary structure of the peptides, the 2D projection of the landscape corresponds to the Ramachandran plot, where it can be seen that the minimum lies in the β-sheet region.

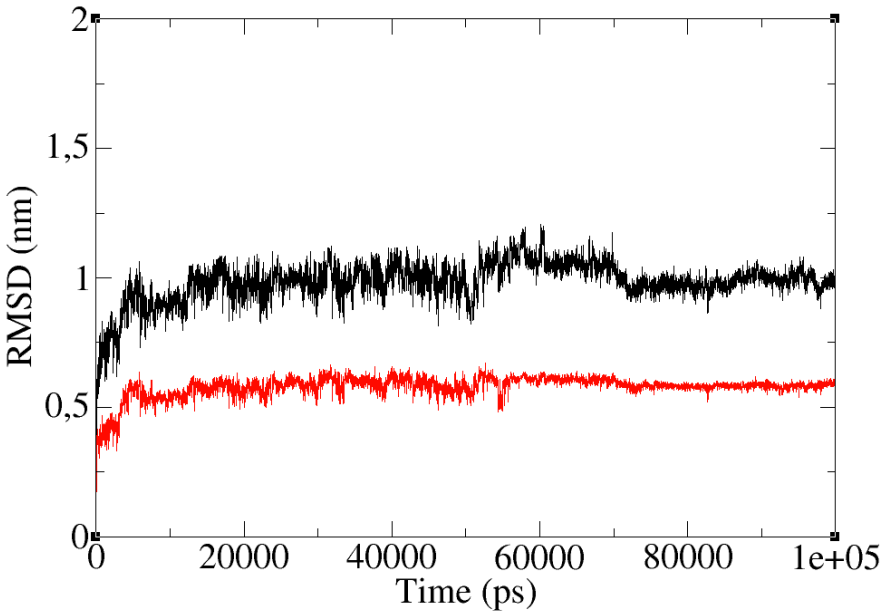

Figure S3: dRMSD for the lateral association (I). The black line corresponds to that of the same color in **Fig. 1** of the main text (*out-of-register* binding mode), representing the standard RMSD. The dRMSD is shown in red, which displays a lower value but the same trend as expected. As in **Fig. 1**, the dRMSD is calculated with respect to the time-zero structure.

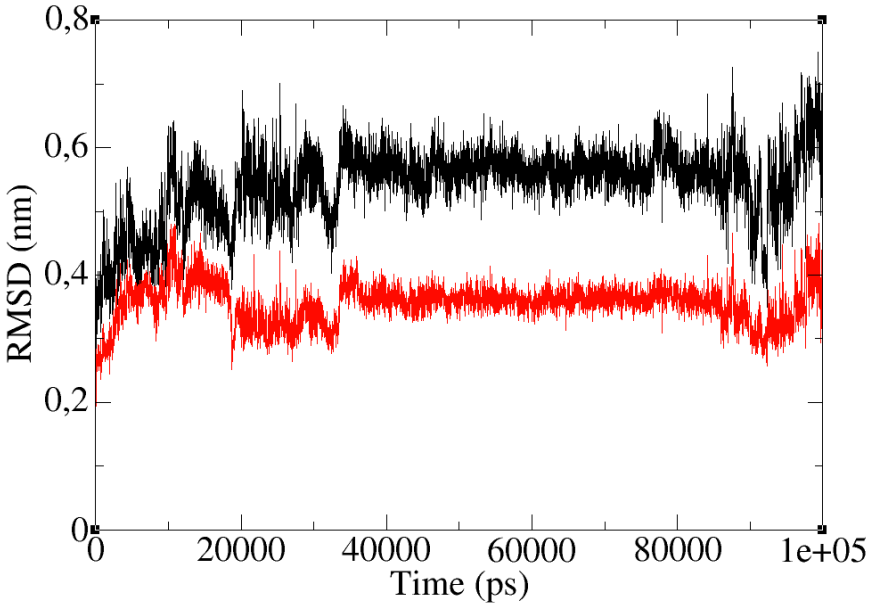

Figure S4: dRMSD for the lateral association (II). The **black** line corresponds to the RMSD of the first *in-register* binding mode simulation (red curve of **Fig. 1** in the main text). As in **Fig. S3**, the red color is that of the dRMSD and the calculations are performed with respect to the time-zero structures.

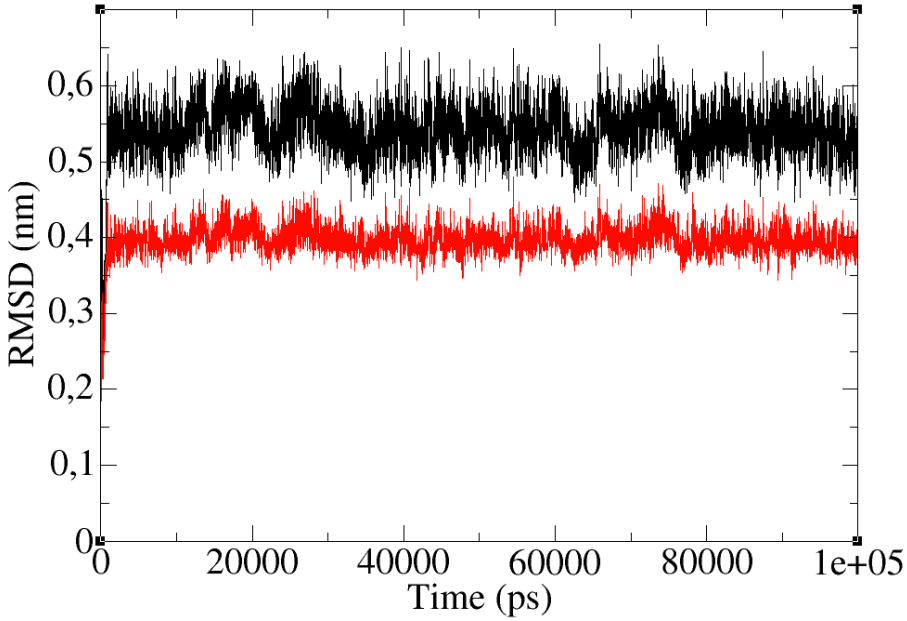

Figure S5: dRMSD for the lateral association (III). The **black** line corresponds to the RMSD of the second in-register binding mode simulation (green curve of **Fig. 1** in the main text). The related dRMSD analysis is shown here in red, as in Fig. **S3**. Again, all the calculations were performed with respect to the time-zero structures.

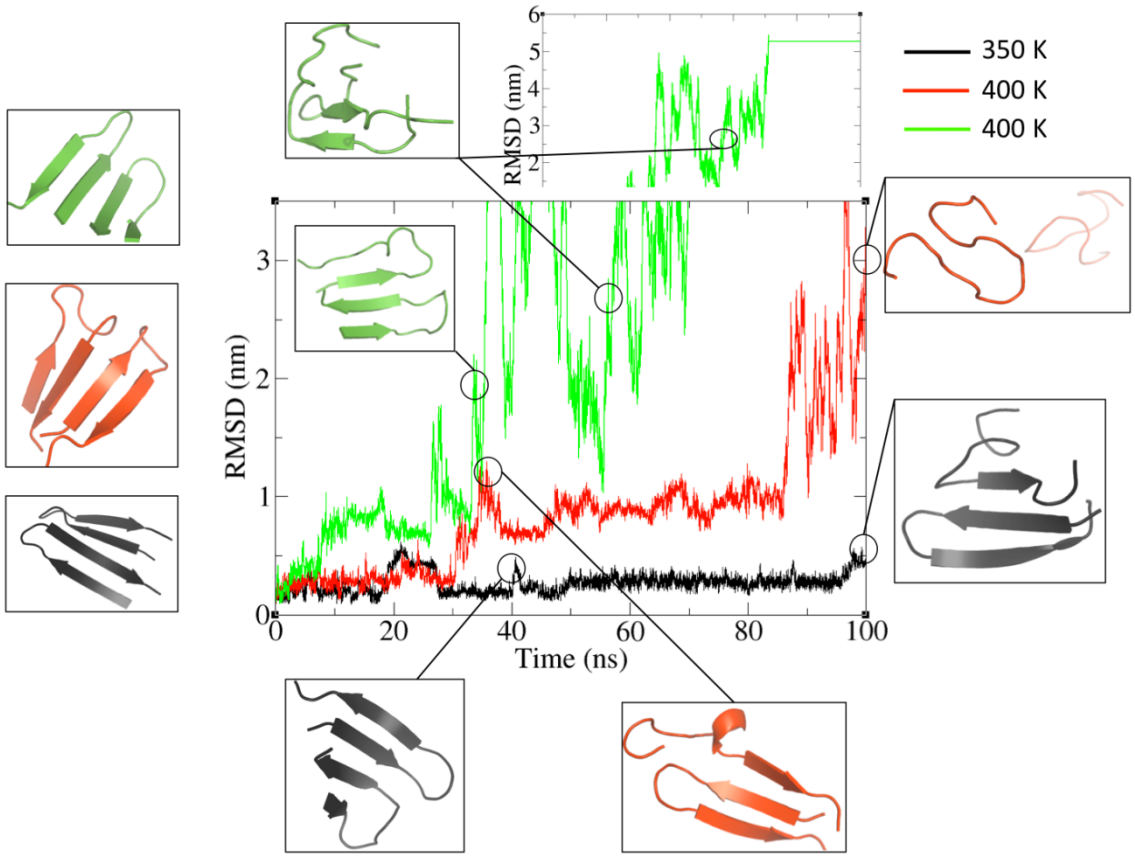

Figure S6: *In-Silico* thermal stability. Trajectories from simulations at high temperature revealing unfolding preferences. The starting structures are depicted on the far left, whereas intermediate and final snapshots are illustrated with circles corresponding to the frames where the snapshots were taken. The RMSD profiles were calculated with respect to the corresponding time-zero structures.

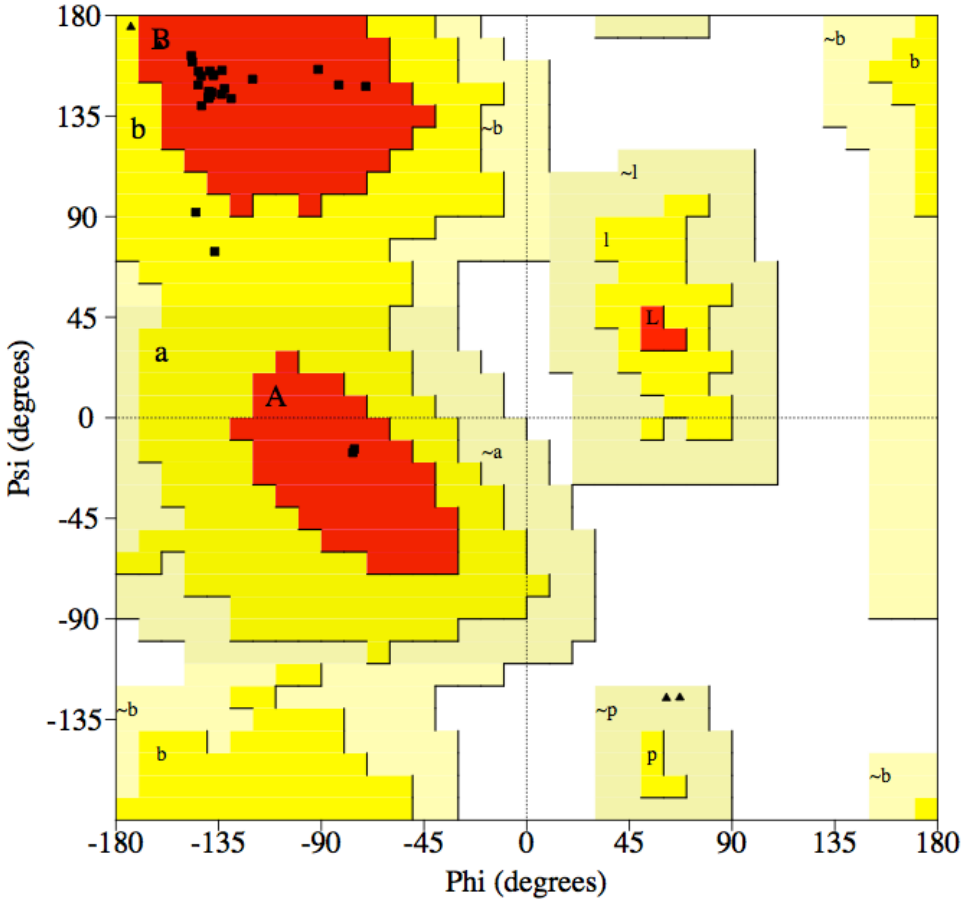

Plot statistics

Residues in most favoured regions [A,B,L]	22	91.7%
Residues in additional allowed regions [a,b,l,p]	2	8.3%
Residues in generously allowed regions [~a,~b,~l,~p]	0	0.0%
Residues in disallowed regions	0	0.0%
	----	------
Number of non-glycine and non-proline residues	24	100.0%
Number of end-residues (excl. Gly and Pro)	2	
Number of glycine residues (shown as triangles)	6	
Number of proline residues	2	

Total number of residues	34	

Based on an analysis of 118 structures of resolution of at least 2.0 Angstroms and R-factor no greater than 20%, a good quality model would be expected to have over 90% in the most favoured regions.

Figure S7: PROCHECK structure validation. A representativeTDP-43(341-357) dimer found in the MD simulations was subjected to stereochemical structure validation. The statistical analysis revealed that 91.7% of the residues are in the most favored region and the remaining 8.3% are also plausible. None of the residues are found in regions generously allowed or disallowed regions. The PROCHECK criterion for a structure to be valid is that at least 90% of the residues have to be present in the most favored regions, which is fulfilled for this system.

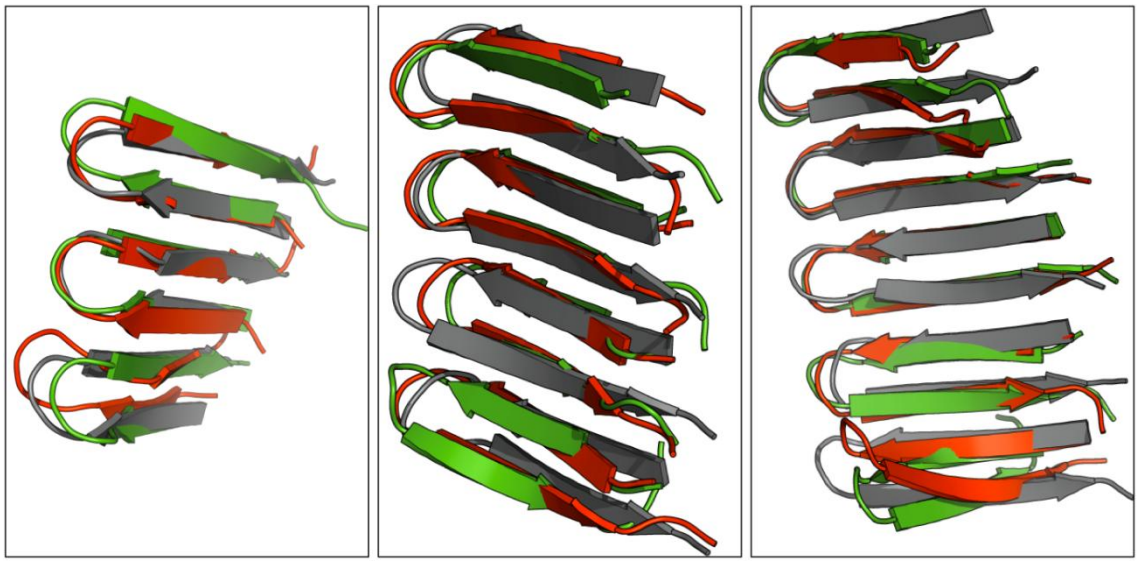

Figure S8: Structural stability of the TDP-43(341-357) oligomers. Structural stability of a TDP-43 (341-357) trimer (*left panel*), tetramer (*central panel*) and pentamer (*right panel).* Snapshots from the oligomers at time 0 (**grey**), 50 (red) and 90 ns (green) from each trajectory. Alignment and superposition of these structures highlight their stability over the course of the 100 ns simulations.

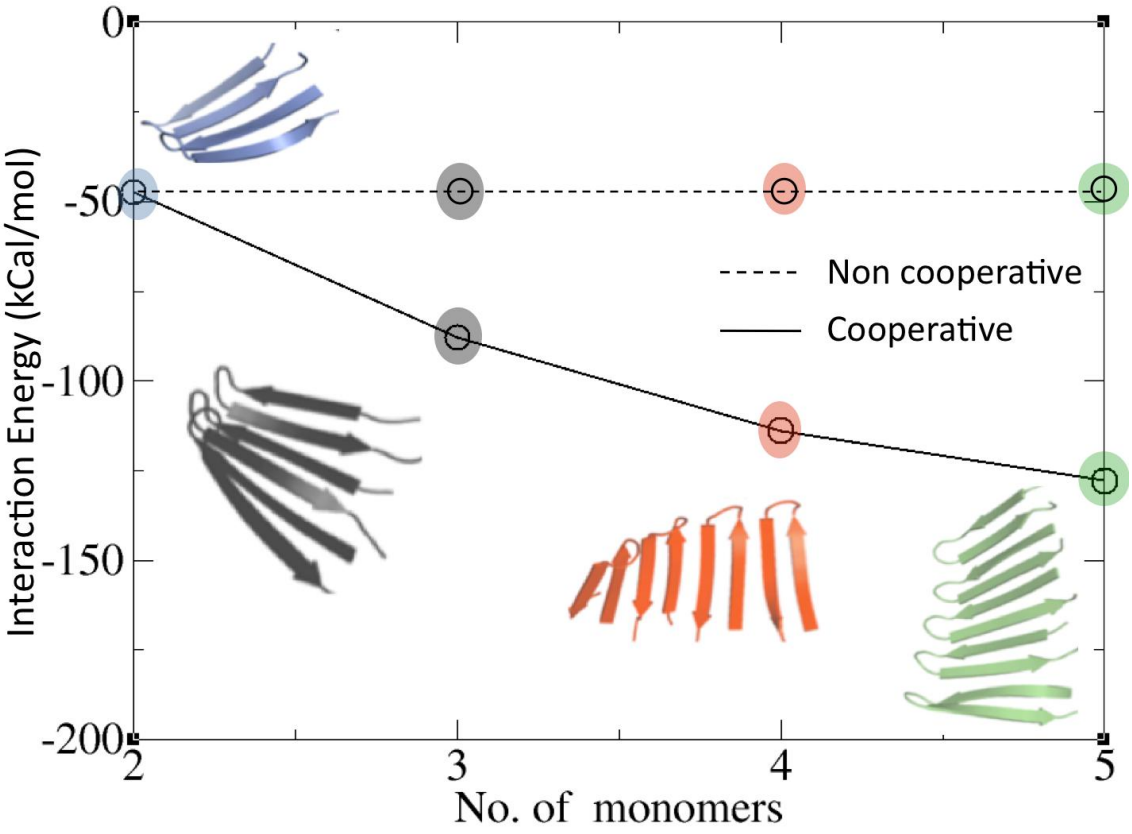

Figure S9: Cooperative hydrogen bonding formation. The interaction energy for two to five TDP-43(341-357) β-hairpins is shown. If the lateral association process associated to fibril formation were not cooperative, then the energy released by oligomerization would be less than the linearly expected, and this is shown in the black line. Each system (dimer, trimer, tetramer and pentamer) is represented in a color code (blue, black, red, and green, respectively). For the sake of clarity, their corresponding energy values are indicated with the same color within the plot. These values are shown in Sup. Table 3.

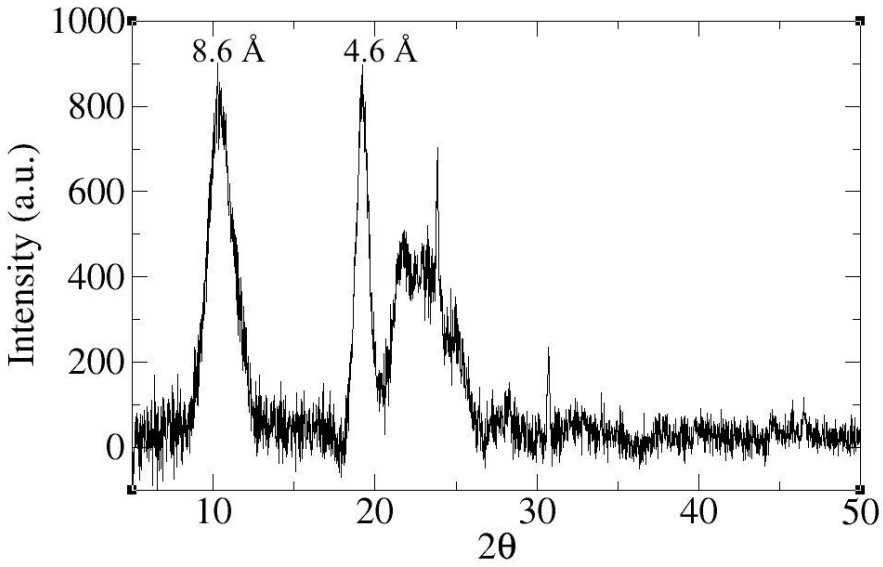

Figure S10: TDP-43(341-357) X-Ray fiber diffraction (XRFD). The X-ray diffraction pattern of preformed fibrils shows the same distances that were observed in the crystal pattern, corresponding to the space between two β-strands in the same β-sheet and between two facing β-strands in different β-sheets facing each other at the dry interface.

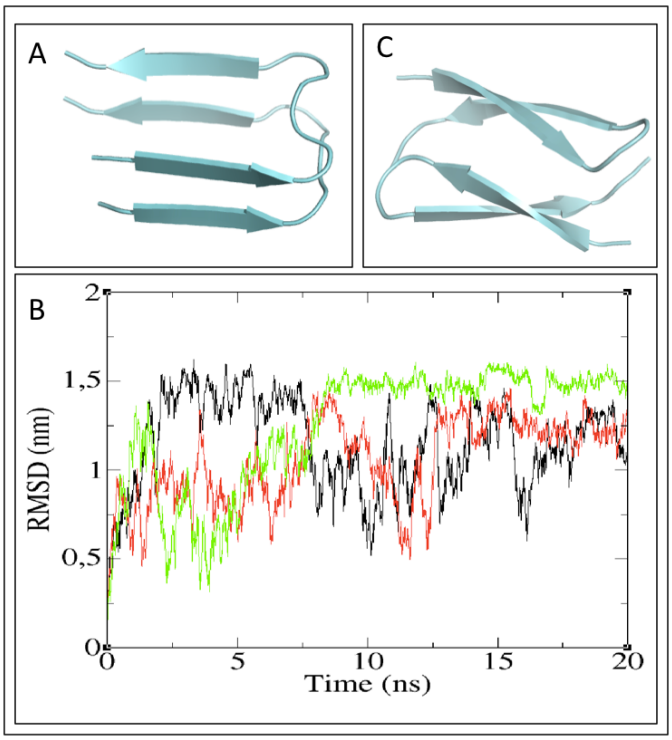

Figure S11: β-arc and β-turn topologies. (**A**) In the "β-arc" topology each TDP-43(341-357) β-hairpin contributes one β-strand to two different β-sheets. Formation of a dry interface restrained to this topology involves longer loops and as a result, significant structural distortion occurs and RMSD values as high as 1.5 nm are reached after only 20 ns, as represented in panel (**B**) Each line (**black**, **green**, and **red**) corresponds to an independent simulation with the same starting configuration (represented in panel (**C**)) but different initial velocities. All the RMSD curves were calculated with respect to the corresponding time-zero structures. (**C**) In contrast, β-hairpin formation is facilitated by the presence of a Gly-Pro turn. In this "β-turn" topology each β-hairpin associates in parallel to contribute two β-strands to the same β-sheet. The structural stability of this motif as the kernel of TDP-43(341-357) aggregation is addressed throughout the main text.

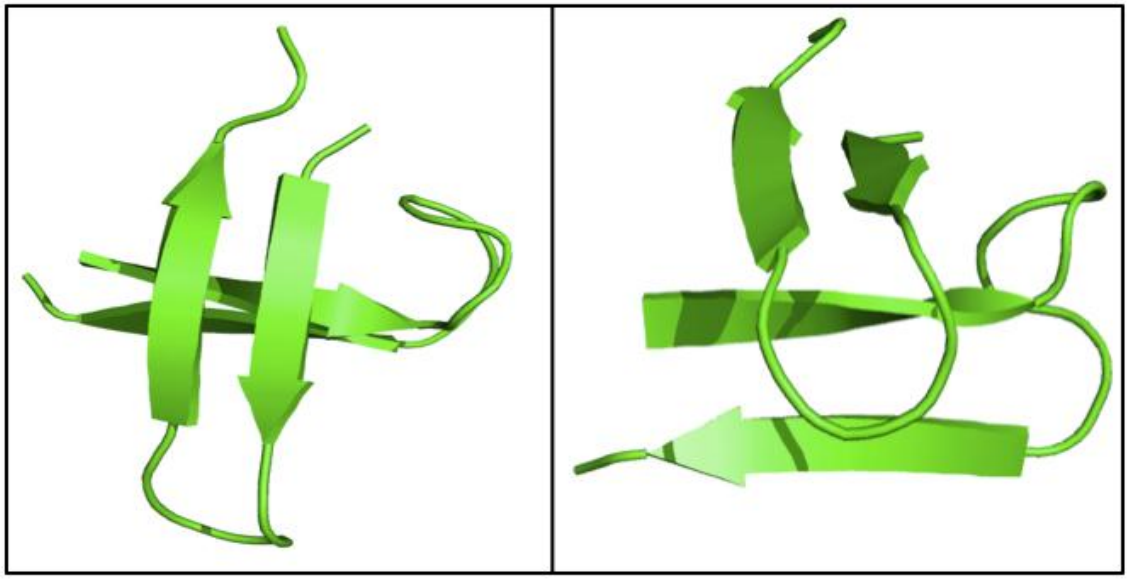

Figure S12. Initial Configuration used in the Simulations. Two different views of two beta-hairpins stacked with an antiparallel orientation with respect to each other at ~ 4.5 - 5 Å, as we observed this inter-strand backbone distances by X-ray diffraction. This set up allows for beta-sheet formation within 100 ns MD simulations.

Supporting Tables

Supplementary Table S1:

Peptides Derived from TDP-43 and Reported to Form Aggregates

Study's Reference	Residue # in TDP-43	Techniques Utilized	Main Results
Guo, W....Wu JY et al (2011) Nat. Struct. Mol. Biol. 18:822-831	286-331 & variant with A315T	ThT, AFM, EM, gel filtration, cytotoxicity assays,	Forms an amyloid-like fibril that is neurotoxic. The A315T mutation enhances fibril formation and toxicity.
Zhu L....Wu, JY Et al. (2014) Hum. Mol. Genetics 23:6863-6877	286-331 & variant with A315T	EM, AMF, ThT, CD, NMR, in cell fluorescence	M307-N319 would adopt a β-strand that packs in an antiparallel fashion. The A315T variant causes the protein's in cell localization to change. This variant can promote the aggretation of Abeta1-40
Liu GCH ...Huang JJT (2013) Chem. Comm. 49:11212-4	287-322, 292-322, 297-322, 302-322, 307-322, 307-322sc, 312-322	EM, CD, vesicle disruption assay	Peptides 287-322, 292-322, 297-322, 302-322, 307-322, but not 312-322 form amyloid-like fibrils. 307-322, but not scrambled 307-322 can induce the aggregation of full length TDP-43
Sun CS … Huang JJT et al. (2014) PloS One 9: e103644	287-322 and variants: G294A, G294V, G295S, G294P, G294,5,6P, G208,9,10P	EM, CD, ThT, FT-Raman, cytotoxicity assays	287-322 and its variants G294A, G294V, G295S form amyloid-like fibrils. The formation of fibrils is reduced or completely disrupted in the other variants.
Jiang et al. (2013) J. Biol. Chem. 288:19614-19624	318-343	ThT fluorescence, CD, NMR, electrophoresis,	Segments 321-330 and 335-343 said to form transient helices which would later convert into beta-hairpins that pack in an anti-parallel fashion.
Wang YT... Yuan HS et al (2013) J. Biol. Chem. 288:9049-9057	208-414	SAXS, EM, CD, ThT	Truncated the RRM2 domain + C-terminal region. Propose that 2 beta strands from this cut RRM2 domain could form amyloid, thereby disrupting the native dimeric structure of TDP-43, which is due to a head/head interaction of the N-terminal domains.
Chen et al. (2010) JACS 132:1186-1187	287-322, 321-353, 351-383, 381-414	EM, CD, ThT, Cytotoxicity Assay	287-322 forms amyloid-like fibrils as do its variants A315T & G294A. The other peptides form amphorous aggregates. Note that the segment studied by us (341-357) would be divided between 2 of the peptides studied by Chen et al. and therefore it is not surprising that this region does not aggregate.

Saini A & Chauhan VS (2011) ChemBioChem 12:2495-2501	15 12-mer peptides spanning TDP-43 residues 220-414. Then 13 peptides derived from TDP-43 segments 246-258 and 311-328	EM, ThT	Found that segments 246-255 and 311-320 can form amyloid-like fibrils that enhance ThT fluorescence. In their peptides, the key 341-357 would have been split into two different peptides (337-349/ 340-362)
Saini A & Chauhan VS Langmuir (2014) 30:3845-3856	Small peptides derived from TDP-43 346-355 and 311-320	EM, CD, Theology, light scattering	Found that 246-255 and its smaller fragment DLII, and 311-320 and its smaller fragment NFGAF can form amyloid-like fibrils and hydrogels.

Supplementary Table S2:

Secondary Structure from Analysis of Circular Dichroism Spectra of TDP-43 341-357 peptides at 25 ºC, pH 6.8 utilizing the CDSSTR algorithm (of the three programs used, CDSSTR yielded the best fits to the experimental spectra).

% Secondary Structure	Day 0		Day 6	
	Ref. Set 4	Ref. Set 7	Ref. Set 4	Ref. Set 7
α-helix	16	23	5	3
β-sheet	28	23	36	33
turn	25	19	24	17
random coil	32	36	33	47
RMSD	0.03	0.03	0.04	0.04

Supplementary Table S3:

X-Ray diffraction reflections in known amyloid and amyloid-like fibrils.

Polypeptide	axial reflection Å (intra- β-sheet)	equatorial reflection Å (inter- β-sheet)	Ref.
TDP-43 (341-357)	4.6	8.6	This work
polyQ	4.7	8.2	(15)
Abeta	4.7	10	(16)
Abeta	4.7	10.4	(17)
α-synuclein	4.7	10 – 11	(18)
Adenovirus fibril	4.8	11.1	(19)
β2-microglobulin	4.8	11.7	(20)
CPEB (*Aplysia*)	4.8	10.7	(21)
Insulin	4.8	9.6	(22)
PI3-SH3	4.7	9.4	(23)
Sup35	4.7	10	(24)

Supplementary Table S4: Interaction energy values, related to **Fig. S9**. The coordinates of the different systems were obtained from the time-averaged structure of largest oligomer (*i.e.*, the pentamer) over a 100 ns MD simulation (See **Fig. 2B** of the main text). The energy values reported correspond to systems that were relaxed by restraining the Cα positions to their experimental interstrand distance values of 4.6 Å. The interaction energies for each system were obtained from the AM1 energy values of the dimer, trimer, tetramer, and pentamer, with respect to the energy of a monomer times the number of monomers in each oligomer.

No. of monomers	ΔE_{int} **(kcal/mol)**
2	-47.34
3	-87.80
4	-113.86
5	-127.87

Supporting References

1. Johnson WC (1999) Analyzing protein circular dichroism spectra for accurate secondary structures. *Proteins* 35, 307-312.

2. Whitmore L, Wallace BA (2008) Protein secondary structure analysis from circular dichroism spectroscopy: methods and reference databases. Biopolymers 89, 392-400.

3. Whitmore L., Wallace BA (2004) DICHROWEB, an online server for protein secondary structure analyses from circular dichroism spectroscopic data. *Nucleic Acids Res* 32:W668-673.

4. Lindorff-Larsen K, Piana S, Palmo K, Maragakis P, Kepleis JL, Dror RO, Shaw DE (2010) Improved side-chain torsion potentials for the Amber ff99SB protein force field. *Proteins* 78, 1950.

5. Hess B, Kutzner C, van der Spoel D, Lindahl E (2008) GROMACS 4: Algorithms for highly efficient, load-balanced, and scalable molecular simulation. *J Chem Theory Comput* 4, 435-447.

6. Berhanu WM, Hansmann UHE (2012) Side-chain hydrophobicity and the stability of Abeta 16-22 aggregates. *Protein Science* 21, 1837-1848.

7. Mompeán M, González C, Lomba E, Laurents DV (2014) Combining Classical MD and QM calculations to elucidate complex system nucleation: a twisted, three-stranded, parallel β-sheet sedes amyloid fibril conception. *J Phys Chem B* 118, 7312-6.

8. Jorgensen WL, Chandrasekhar J, Madura JD, Impey RW, Klein ML (1983) Comparison of simple potential functions for simulating liquid water. *J Chem Phys* 79, 926-935.

9. Berendsen HJC, Postma JPM, van Gunsteren WF, DiNola A, Haak JR (1984) Molecular dynamics with coupling to an external bath. *J Chem Phys* 81:3684.

10. Nosé S (1984) A molecular dynamics method for simulations in the canonical ensemble. *Mol Phys* 52, 255-268.

11. Parrinello M, Rahman A (1981) Polymorphic transitions in single crystals: a new molecular dynamics method. *J Appl Phys* 52, 7182.

12. Hess B, Bekker H, Berendsen HJC, Fraaije JGEM (1997) LINCS: A linear constraint solver for molecular simulations. *J Comput Chem* 18, 1463-1472.

13. Darden T, York D, Pedersen L (1993) Particle mesh ewald: an N·lon(N) method for Ewald sums in large systems. J. Chem. Phys. 98, 10089-10092.

14. Dominguez C, Boelens R, Bonvin AMJJ (2003) HADDOCK: a protein-protein docking approach based on biochemical and/or biophysical information. *J Am Chem Soc* 125, 1731-1737.

15. Sharma D, Shinchuk LM, Inouye H, Wetzel R, Kirschner DA (2005) Polyglutamine homopolymers having 8-45 residues form slablike beta-crystallite assemblies. *Proteins* 61, 398-411.

16. Petkova AT, Buntkowsky G, Dyda F, Leapman RD, Yau WM, Tycko R (2004) Solid state NMR reveals a pH-dependent antiparallel beta-sheet registry in fibrils formed by a beta-amyloid peptide. *J Mol Biol* 335, 247-60.

17. McDonald M, Box H, Bian W, Kendall A, Tycko R, Stubbs G (2012) Fiber diffraction data indicate a hollow core for the Alzheimer's Aβ 3-fold symmetric fibril. *J Mol Biol* 423, 454-61.

18. Serpell LC, Berriman J, Jakes R, Goedert M, Crowther RA (2000) Fiber diffraction of synthetic alpha-synuclein filaments shows amyloid-like cross-beta conformation. *Proc Natl Acad Sci USA* 97, 4897-902.

19. Papanikolopoulou K, Schoehn G, Forge V, Forsyth VT, Riekel C, Hernandez JF, Ruigrok RW, Mitraki A (2005) Amyloid fibril formation from sequences of a natural beta-structured fibrous protein, the adenovirus fiber. *J Biol Chem* 280, 2481-90.

20. Ivanova MI, Sawaya MR, Gingery M, Attinger A, Eisenberg D (2004) An amyloid-forming segment of beta2-microglobulin suggests a molecular model for the fibril. *Proc Natl Acad Sci USA* 101, 10584-9.

21. Raveendra BL, Siemer AB, Puthanveettil SV, Hendrickson WA, Kandel ER, McDermott AE (2013) Characterization of prion-like conformational changes of the neuronal isoform of Aplysia CPEB. *Nat Struct Mol Biol* 20, 495-501.

22. Choi JH, May BC, Wille H, Cohen FE (2009) Molecular modeling of the misfolded insulin subunit and amyloid fibril. *Biophys J* 97, 3187-95.

23. Ghahghaei A, Faridi N (2009) Review: structure of amyloid fibril in diseases. *J BioMed Sci Eng* 2, 345-358.

24. Balbirnie M, Grothe R, Eisenberg DS (2001) An amyloid-forming peptide from the yeast prion Sup35 reveals a dehydrated beta-sheet structure for amyloid. *Proc Natl Acad Sci USA* 98, 2375-80.

Complete citation of Gaussian 09

Gaussian 09, Revision D.01, Frisch, M. J.; Trucks, G. W.; Schlegel, H. B.; Scuseria, G. E.; Robb, M. A.; Cheeseman, J. R.; Scalmani, G.; Barone, V.; Mennucci, B.; Petersson, G. A.; Nakatsuji, H.; Caricato, M.; Li, X.; Hratchian, H. P.; Izmaylov, A. F.; Bloino, J.; Zheng, G.; Sonnenberg, J. L.; Hada, M.; Ehara, M.; Toyota, K.; Fukuda, R.; Hasegawa, J.; Ishida, M.; Nakajima, T.; Honda, Y.; Kitao, O.; Nakai, H.; Vreven, T.; Montgomery, J. A., Jr.; Peralta, J. E.; Ogliaro, F.; Bearpark, M.; Heyd, J. J.; Brothers, E.; Kudin, K. N.; Staroverov, V. N.; Kobayashi, R.; Normand, J.; Raghavachari, K.; Rendell, A.; Burant, J. C.; Iyengar, S. S.; Tomasi, J.; Cossi, M.; Rega, N.; Millam, M. J.; Klene, M.; Knox, J. E.; Cross, J. B.; Bakken, V.; Adamo, C.; Jaramillo, J.; Gomperts, R.; Stratmann, R. E.; Yazyev, O.; Austin, A. J.; Cammi, R.; Pomelli, C.; Ochterski, J. W.; Martin, R. L.; Morokuma, K.; Zakrzewski, V. G.; Voth, G. A.; Salvador, P.; Dannenberg, J. J.; Dapprich, S.; Daniels, A. D.; Farkas, Ö.; Foresman, J. B.; Ortiz, J. V.; Cioslowski, J.; Fox, D. J. Gaussian, Inc., Wallingford CT, 2009.